Short Circuit Network Equivalents of Systems with Inverter-based Resources

R. M. Furlaneto, I. Kocar, A.Grilo-Pavani, U. Karaagac, A. Haddadi, and E. Farantatos

Abstract— **Large transmission networks are often represented with short circuit network equivalents to share with neighboring utilities and distribution providers. The computation of network equivalents for short circuit studies is straightforward in systems predominantly based on conventional synchronous generators (SGs). However, the integration of renewable powered plants such as solar and wind parks (WPs) introduces inverter-based resources (IBRs) in the grid with different and nonlinear fault current characteristics. The increasing share of IBRs changes the way power systems respond during disturbances. The application of conventional approach to obtain network equivalents based on the computation of Thevenin equivalent at the point of interest to systems with high share of IBRs will result in misleading short circuit calculations. This paper is the first step in the identification of active nonlinear network equivalents for short circuit studies in systems with IBRs. A new concept of voltage dependent network equivalents (VDNEs) is proposed. Considering the increasing complexity of networks with several and different type of IBR installations, a measurement-based approach using simulated fault currents is proposed to obtain VDNEs. The short-circuit response of VDNEs are validated considering a network with WPs consisting of Type-IV/Full-Size Converter (FSC) wind turbine generators (WTGs).**

Keywords—Inverter-based resources, full-scale converter, Type-IV wind turbine generator, network equivalents, short circuit calculation, faults.

I. INTRODUCTION

A network equivalent for short circuit studies represents a large transmission network by a voltage source behind impedance. Network equivalents facilitate sharing network data with neighboring utilities and distribution companies. Their computation is straightforward and well documented for systems where conventional synchronous generators (SGs) are the principal source of generation. However, the increasing share of inverter-based resources (IBRs) in grids requires revising the way network equivalents are defined.

IBRs include solar plants and wind parks (WPs) employing Type-III (Doubly Fed Induction Generator, DFIG) and Type-IV (Full-Size Converter, FSC) wind turbine generators (WTGs). Their fault response is different from conventional SGs and depends largely on control schemes of voltage source converters (VSCs) employed in wind turbine generators

(WTGs) or solar inverters [1]-[6]. For steady-state calculations, they are represented with nonlinear voltage dependent current sources in the positive sequence network. This approach has been demonstrated to successfully match detailed Electromagnetic Transients-type (EMT-type) models in steady state [2]-[4] as long as the current source is computed according to the control schemes of VSCs, current limiters and other limiters.

Transient models of IBRs have been central in recent research contributions for the validation of simplified short-circuit models and to understand the impact of IBRs on system protection [7]-[18]. There is also an interest in obtaining their equivalents in the sequence domain for short circuit studies. However, there is no work on the identification of network equivalents for systems with high share of IBRs to be used in short circuit studies.

The objective of this paper is to develop a network equivalent representing the steady-state short circuit response of a system with high share of IBRs. The increasing number of IBR installations and the existence of different control schemes and IBR types increase the complexity of modern grids and their short circuit characteristics. The classical Thevenin equivalent may no longer be adequate for representing such short-circuit characteristics, depending on system strength and integration level of IBRs. To address this challenge, this work proposes a quantitative approach for the identification of network equivalents using simulation-based fault measurements.

The proposed equivalent circuit is a voltage dependent network equivalent (VDNE) consisting of a voltage source behind impedance that accounts for conventional SGs in the network, in parallel with a voltage-dependent current source accounting for IBRs in the system. The nonlinear current source is parameterized through short-circuit current measurements obtained under varying fault impedance values.

The effectiveness of the proposed VDNE is demonstrated through simulation studies conducted on a multi-WP test system. Validation studies are performed against detailed EMT simulations considering the steady state short circuit response and with varying fault impedances and X/R ratios of the external grid. WPs employing FSC WTGs with regulation only

---

R. M. Furlaneto and A. Grilo-Pavani are with the Federal University of ABC, Santo Andre, Brazil (e-mails: renan.furlaneto@aluno.ufabc.edu.br; ahda.pavani@ufabc.edu.br)

I. Kocar is with the Department of Electrical Engineering, Polytechnique Montréal, QC H3T 1J4, Canada (e-mail: ilhan.kocar@polymtl.ca).

U. Karaagac is with the Department of Electrical Engineering, Hong Kong Polytechnic University, HKSAR (e-mail: ulas.karaagac@polyu.edu.hk)

Evangelos Farantatos and Aboutaleb Haddadi are with EPRI, USA (emails: efarantatos@epri.com; ahaddadi@epri.com)

on positive sequence currents are considered as a first step; future work includes extending the proposed VDNE to incorporate flexible negative sequence behavior as well.

The computation of short circuit currents using the proposed network equivalent model requires iterative calculation owing to the nonlinear behavior of IBRs. This nonlinear characteristic is accounted for by employing a voltage-dependent current source element.

This paper is organized as follows. Section II gives an overview of IBR models in the literature for steady-state short circuit studies. Section III describes the proposed methodology for identifying network equivalents and its use in short circuit current computations. Section IV gives numerical results and validations with detailed EMT simulations. A multi-WP system is considered for validation studies. Section V is the conclusions.

II. Overview of IBR Modeling in Short Circuit Studies

A. Short Circuit Modeling of Wind Turbine Generators

In a typical WP, the power produced by the WTGs is transmitted to the point of interconnection (POI) through a medium voltage (MV) collector grid and a WP transformer as shown in Fig. 1. The WP transformer is usually equipped with an on-load-tap-changer to keep the MV collector bus voltage close to its nominal value. According to customary grid code requirements, the WP should have a central controller at the WP substation to control the reactive power, voltage, or power factor at the POI.

Aggregated modeling is often favored for faster simulations in EMT-type simulation packages. It is considered to provide sufficiently accurate results for short circuit studies on the grid side or load flow studies [19]. In this modeling approach, WTGs, and step-up turbine transformers to the medium voltage (MV) collector grid are aggregated. The collector grid is represented with an equivalent collector grid.

Like conventional SGs, a single or aggregated WTG is also modeled with PQ constraints in load flow studies. However, modeling of WTGs in short circuit studies is quite different from the modeling of SGs. VSCs are the essential grid-integration component of WTGs [20]. The short circuit response of WTGs depends on the control schemes and limiters of the VSCs [1]-[6].

An accepted modeling approach for WTGs in steady-state short circuit analysis is to represent them with voltage controlled current source [21] as shown in Fig. 2. This current source is nonlinear due to current limiters and other limiters in the control. Its active and reactive components in the sequence domains largely depend on the control scheme employed in VSCs. The transient period following the fault inception is very short for FSC topology, i.e., typically under 1 cycle. For DFIG topology these periods are longer since the machine is not decoupled from the network and its dynamics play a role in the establishment of the steady state short circuit response.

The generic EMT model of the FSC topology used in this paper is detailed in [22]. This model has been used for validations in the development of steady state short circuit models [2]-[4] transferred to commercial protection packages

such as ASPEN and CAPE. In this work, the model is set to give priority to reactive current and provide additional reactive current as shown in Fig. 3 during voltage disturbances per a grid code requirement [23].
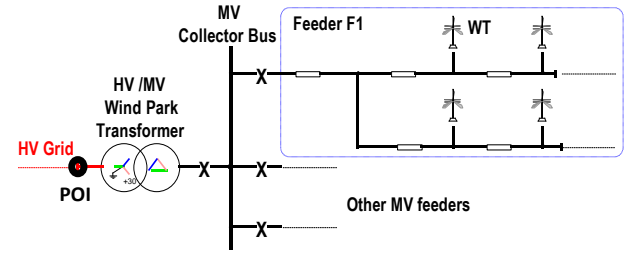

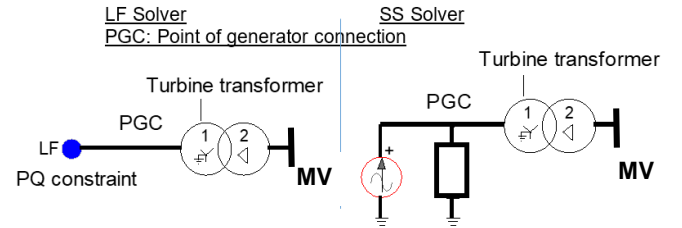Fig. 1 Single Line diagram of a typical WP

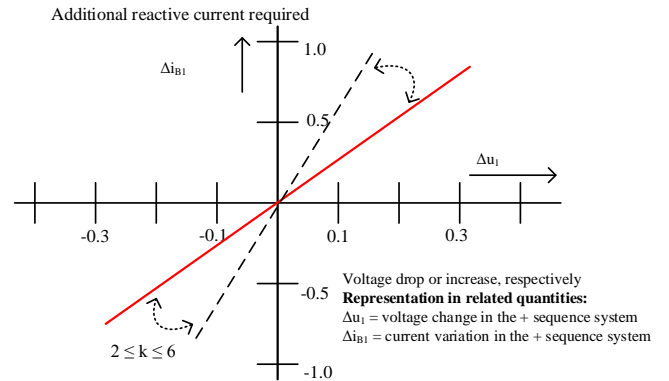Fig. 2 Steady state models of WTGs for load flow and short-circuit studies

Fig. 3 Wind turbine reactive output current during voltage disturbances [23]

III. Network Equivalent and Short-Circuit Calculations

A. Voltage Dependent Network Equivalent

Consider a 315 kV system with two WPs as shown in Fig. 4 connected to an external grid through a line at the location abbreviated as POE which stands for the point of network equivalent. This network is a simplified version of the Gaspésie peninsula network described in [24] which is experiencing a massive wind energy integration. The objective is to find the equivalent of the network that consists of two WPs and two conventional sources. Note that, when there is a fault at the POE, the fault current contribution of WPs is more than 10% in the test case considered. Per IEC 60909-0-2016, power station units with full size converter may be neglected if their contributions are not higher than 5% of the initial short circuit without these power station units.

The equivalent network considered in this paper is the positive sequence network. In negative sequence, the representation of WPs depends on many factors including the

type of WTGs, control schemes and measurement filters. Ideally, the grid side converter (GSC) control of FSC with a positive sequence control scheme is not expected to inject any negative sequence current to the grid during unbalanced loading conditions or faults [8]. On the other hand, its terminal voltage contains negative sequence components and due to the phase shift introduced by measurement filters a small amount of negative sequence current can circulate in the WTG [3]. It is possible to represent this with a large impedance in the negative sequence system although its overall impact on the network equivalent will be negligible.

When it comes to DFIG topology or FSC with decoupled control schemes (DSC), there is a number of factors that affect the behavior of WTG in the negative sequence system including coupling between sequences due to current limiters and control priorities [25]-[28]. A detailed discussion from the point of network equivalents will be provided in a separate work.

In this paper, WPs consisting of FSCs are considered. The regulation is on the positive sequence power. Given that WTGs can be represented with voltage controlled current sources in short circuit studies [3], [21], we posit that networks with large scale integration of WPs can be represented as a combination of a linear voltage source behind impedance and a voltage dependent current source as depicted in Fig. 5. This equivalent network is called VDNE.
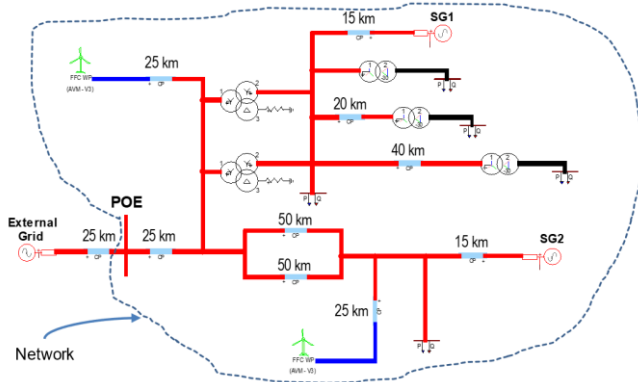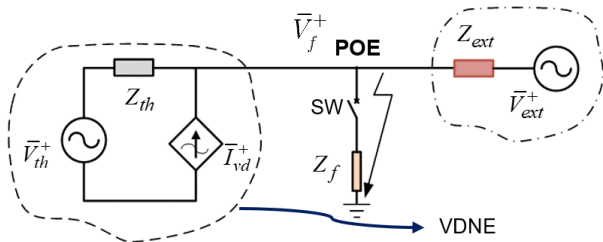

Fig. 4 315 kV Multi-WP System

Fig. 5 Proposition: Voltage dependent network equivalent (VDNE)

In Fig. 5 $\bar{V}_{th}^+$ is the Thevenin equivalent voltage related to the conventional sources in the network. Z_{th} is the complex Thevenin impedance of the linear passive components in the network considering transmission lines, short-circuit impedance of conventional generators, transformers, linearized loads (using load flow solution) and WP circuits (excluding VSCs). Because of the shunt filters at wind turbine terminals

and capacitance of collector grids, the WP circuits have still an impact on the overall value of the Thevenin impedance even if VSCs are excluded. $\bar{I}_{vd}^+$ is a voltage dependent current source to account for the fault contribution of WTGs. Z_f is the fault impedance and $\bar{V}_f^+$ is the fault voltage at the POE. Z_{ext} is the complex Thevenin impedance of the external grid that may take arbitrary values. $\bar{V}_{ext}^+$ is the voltage source behind Thevenin impedance of the external grid. The exact details of the external grid are unknown a priori. The power transfer and pre-fault voltage at the POE are assumed to be known. SW represents an artificial three-phase switch to illustrate a three-phase fault inception. All quantities are positive sequence quantities.

Z_{th} is the impedance of the network seen from the POE and computed using a conventional method based on current injection at the POE and by ignoring VSCs. Beforehand, the network is linearized using the load flow solution, and the ideal voltage sources representing conventional generators are shorted in the network. However, it is important that VSCs are not shorted and kept open circuited, otherwise Z_{th} will be underestimated and short circuit currents will be overestimated. $\bar{V}_{th}^+$ and $\bar{V}_{ext}^+$ are equal to the pre-fault voltage at the POE obtained using load flow solution.

Here the challenge is to identify $\bar{I}_{vd}^+$ as a function of fault voltage across its terminals, i.e., $\bar{V}_f^+$. In this work, a measurement-based approach using simulations is tested. By using the complete network, fault current ($\bar{I}_f^+$) with respect to $\bar{V}_f^+$ is identified by applying a series of short circuits at the POE by varying Z_f. Although the simulations are performed in EMTP, the identification process can be performed efficiently in the phasor domain using a steady-state tool with appropriate IBR models. Here the objective is proof of concept with a tool with established WP models. The voltage source of the external grid in the complete network is the reference and slack bus in load flow solution. The load flow solution is used to initialize EMT simulation. Steady state fault conditions are used to obtain a set of $\bar{I}_f^+$ versus $\bar{V}_f^+$ data. This data is then used to compute $\bar{I}_{vd}^+$ with respect to $\bar{V}_f^+$ in the equivalent circuit given that $\bar{I}_{vd}^+$ is the only unknown in this circuit once the fault current and voltage are specified. Finally, $\bar{I}_{vd}^+$ is parametrically identified (fitted) as a function of $\bar{V}_f^+$ using regression techniques. Two regression methods are considered:

In Method I, the active and reactive components of $\bar{I}_{vd}^+$ are obtained first as follows

$$I_{vd}^{+d} = \cos\varphi\, I_{vd}^{+}$$
$$I_{vd}^{+q} = \sin\varphi\, I_{vd}^{+} \tag{1}$$

where I_{vd}^{+d} and I_{vd}^{+q} are the positive sequence active and reactive current components, respectively, and φ is the angle difference between phasors $\bar{I}_{vd}^{+}$ and $\bar{V}_{f}^{+}$.

These fault current components are then fitted to a polynomial function of the fault voltage magnitude V_{f}^{+}

$$I_{vd}^{+d} = a_{n}\, V_{f}^{+^{n}} + a_{n-1}\, V_{f}^{+^{n-1}} + \dots + a_{0}$$
$$I_{vd}^{+q} = a_{n}'\, V_{f}^{+^{n}} + a_{n-1}'\, V_{f}^{+^{n-1}} + \dots + a_{0}'. \tag{2}$$

where $a_{n}, a_{n-1}, \dots, a_{0}$ and $a_{n}', a_{n-1}', \dots, a_{0}'$ are the polynomial coefficients, and n is the degree of the polynomial function. The coefficients are computed using Vandermonde method [29]. The order of polynomials is taken as 2 or 3 to minimize the fitting error.

In Method II, $\bar{I}_{vd}^{+}$ is separated into its real and imaginary parts to see their relationship with $\bar{V}_{f}^{+}$, as a set of two-variable functions given as follows

$$\mathrm{Re}(\bar{I}_{vd}^{+}) = f(\mathrm{Re}(\bar{V}_{f}^{+}), \mathrm{Im}(\bar{V}_{f}^{+}))$$
$$\mathrm{Im}(\bar{I}_{vd}^{+}) = f(\mathrm{Re}(\bar{V}_{f}^{+}), \mathrm{Im}(\bar{V}_{f}^{+})) \tag{3}$$

Re gives the real part of the phasor whereas Im gives the imaginary part.

Localized weighted regression algorithm (LOWESS) is applied to compute (3). In this technique, polynomial weighted fitting of the data is mainly performed with local observation of data and using least squares method to estimate the errors. The overall data is split into equally distributed windows. Their width is an important parameter to get a smooth fitting. The width or span of the windows is defined in percentage of the data points considered. In this work, the span is adjusted to maintain a sum of squared errors below 0.001.

Note that, (3) needs to be evaluated for each window of data. Once the data windows are specified, regression weights for each data point is computed in each window considering only the data points that lie in the same window. Then, weighted least squares regression is used to fit the sample data points to a polynomial of first degree for each window. Reader can refer to [30] for details on this regression technique.

The reason that LOWESS is chosen in the fitting of real and imaginary parts as opposed to polynomial fitting used in Method I, is that it provides more accurate results in the computation of short circuit currents using VDNE when the fault impedances are complex as will be shown in this paper. Both methods show similar performance in terms of accuracy for faults with purely resistive fault impedances.

Both Methods I and II were implemented using MATLAB software.

B. Use of VDNE for Short Circuit Studies

Once the VDNE is obtained, it can be used to evaluate steady state short circuit in systems with arbitrary external grid characteristics. As $\bar{I}_{vd}^{+}$ is expected to have a nonlinear behavior, an iterative solution will be necessary in most cases, i.e., unless the equivalent network is decoupled from the external grid by a bolted fault, to establish a consistent solution in terms of the nonlinear characteristics of the network equivalent, fault conditions and external grid parameters. A fixed-point approach is detailed below for balanced faults. Fig. 6 shows the flowchart of the iterative solution.
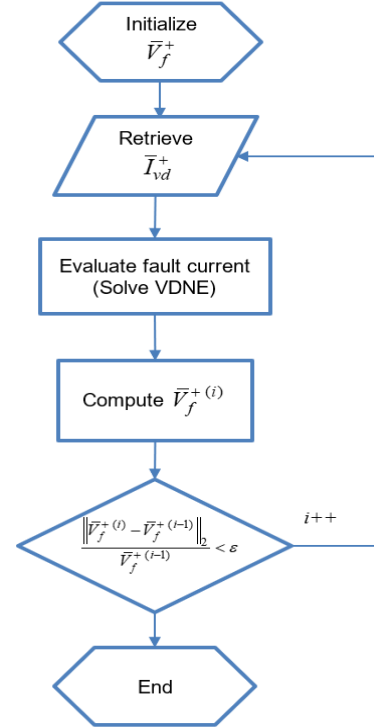

Fig. 6 Flowchart of iterative solution

Following the inception of a three-phase fault, $\bar{I}_{vd}^{+}$ needs to be adjusted iteratively so that it satisfies its voltage dependence function, and the circuit conforms to basic circuit laws. The system of circuit equations is given as follows:

$$\bar{I}_{th}^{+} = \frac{\bar{V}_{th}^{+} - \bar{V}_{f}^{+}}{Z_{th}} \tag{4}$$

where $\bar{I}_{th}^{+}$ is the current contributed by $\bar{V}_{th}^{+}$. $\bar{I}_{ext}^{+}$ is the short circuit component from the external grid side and given by

$$\bar{I}_{ext}^{+} = \frac{\bar{V}_{ext}^{+} - \bar{V}_{f}^{+}}{Z_{ext}} \tag{5}$$

$\bar{V}_{f}^{+}$ is given by

$$\bar{V}_{f}^{+} = Z_{f}\,\bar{I}_{f}^{+} \tag{6}$$

where $\bar{I}_{f}^{+}$ is the fault current given by

$$\bar{I}_{f}^{+} = \bar{I}_{th}^{+} + \bar{I}_{ext}^{+} + \bar{I}_{vd}^{+} \tag{7}$$

The iterative solution used in this work updates $\bar{I}_{vd}^{+}$ using

$\bar{V}_f^+$ calculated by (6). The initial guess of $\bar{V}_f^+$ is done by using the linear components of VDNE $\bar{I}_{vd}^+$ is evaluated as a function of $\bar{V}_f^+$. Every time $\bar{V}_f^+$ is updated using (6), it is necessary to recalculate $\bar{I}_f^+$ using (7) with updated currents. The difference in $\bar{V}_f^+$ between consecutive iterations is used to check convergence. Note that, to calculate the exact contribution of the external grid to the fault, it is necessary to superpose $\bar{I}_{ext}^+$ with its pre-fault current.

IV. NUMERICAL RESULTS

A. Computation of the VDNE Parameters

Consider the test system of Fig. 4.

There are two WPs and each WP contains an aggregated model of 200 WTGs with 1.5 MW of active power rating. Both WPs operate with control on reactive power before the fault inception. EMT simulations are initialized from the load flow solution. Fault currents are measured when steady-state conditions are reached after the fault inception.

To study the concept of VDNE, it is necessary first to identify $\bar{V}_{th}^+$, Z_{th} and $\bar{I}_{vd}^+$.

$\bar{V}_{th}^+$ is equal to $181.34\angle 0.68° \text{ kV}$, this is the rms line-to-neutral pre-fault voltage. It comes from the load flow solution in which the source representing the external grid (behind the 25 km line) is the reference bus. Z_{th} is computed as $42.29\angle 76.59° \text{ }\Omega$. The X/R ratio of Z_{ext} is set to 30 with R equal to $5\text{ }\Omega$. $\bar{I}_{vd}^+$ is a nonlinear function of the fault voltage and is identified using simulation-based measurements.

Fig. 7 and Fig. 8 show rms active and reactive components of $\bar{I}_{vd}^+$ versus fault voltage and their approximations obtained by applying Method I. A sample set of data is provided in TABLE I. Note that positive sign for active component indicates that voltage dependent current source generates active power. On the other hand, it is the negative sign for reactive component that indicates generation of reactive power.

The polynomial functions are given by

$$\begin{cases} I_{vd}^{+d} = 1.11 \times 10^{-12} V_f^{+3} - 1.95 \times 10^{-7} V_f^{+2} \dots \\ \qquad + 8.83 \times 10^{-3} V_f^+ + 682.51 \\ I_{vd}^{+q} = 1.01 \times 10^{-7} V_f^{+2} - 1.33 \times 10^{-2} V_f^+ \dots \\ \qquad - 91.32 \end{cases} \quad (8)$$

Note that the VDNE accounts for both IBRs and conventional sources but $\bar{I}_{vd}^+$ is not necessarily equal to the sum of WP currents at the POI. This is because of the network reduction that transforms the magnitude and angle characteristics of VSC currents through passive components of the network such as transmission lines and transformers.

The WPs respect the control settings by providing additional reactive current as the system voltage goes down, and by reducing the active current component to respect VSC current limits. This is seen in Fig. 9 and Fig. 10 which show active current and reactive current components of WPs with respect to fault voltage. Active current component being positive means that WP generates active power whereas reactive current component being negative means generation of reactive power.

TABLE I
AN EXCERPT OF DATA USED TO IDENTIFY VDNE

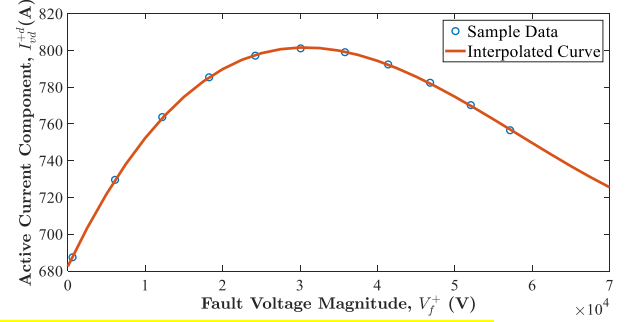| Z_f (Ω)	Fault Voltage kV (Angle)	Active Component A	Reactive Component A
0.1	0.61 (-79.16)	687.46	-100.49
1	6.10 (-78.16)	729.61	-167.00
2	12.20 (-77.01)	763.72	-237.13
3	18.25 (-75.80)	785.39	-299.59
4	24.22 (-74.52)	797.16	-354.06
5	30.08 (-73.18)	801.14	-399.65
6	35.81 (-71.79)	799.05	-436.73
7	41.39 (-70.36)	792.38	-466.00
8	46.81 (-68.90)	782.43	-488.67
9	52.06 (-67.44)	770.26	-506.14
10	57.15 (-65.98)	756.58	-519.62

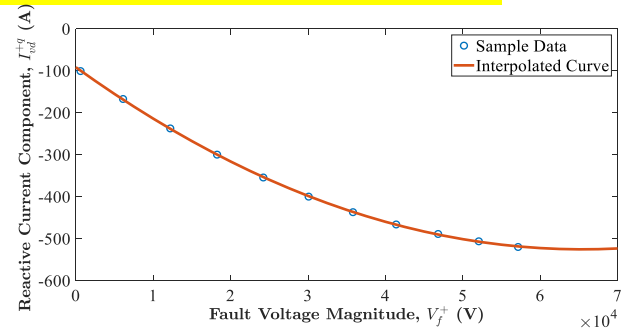Fig. 7 Active current component of $\bar{I}_{vd}^+$ versus fault voltage

Fig. 8 Reactive current component of $\bar{I}_{vd}^+$ versus voltage
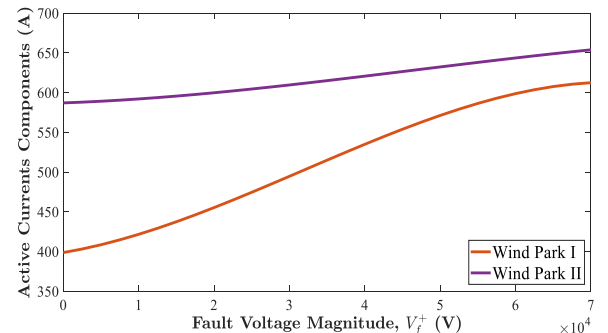

Fig. 9 Active current components of WPs versus fault voltage

Fig. 11 and Fig. 12 show the active and reactive current components of both WPs versus voltage magnitude at their POI.
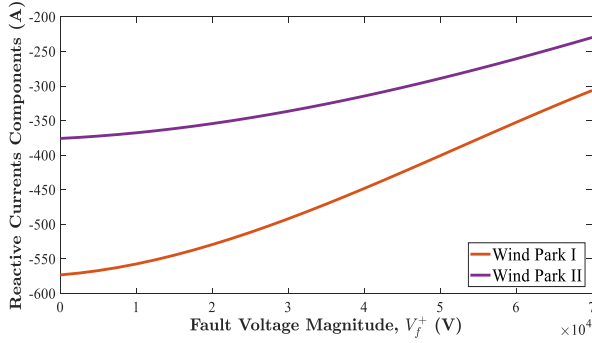

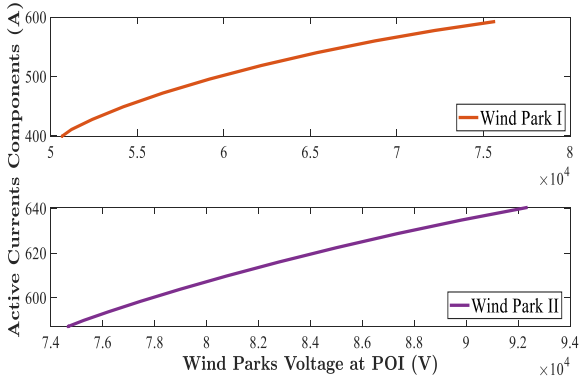Fig. 10 Reactive current components of WPs versus fault voltage

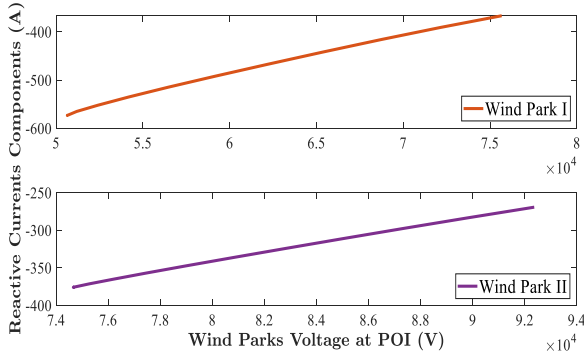Fig. 11 Active current components of WPs versus voltage at their POI

Fig. 12 Reactive current components of WPs versus voltage at their POI

The surfaces seen in Fig 13 and Fig 14 are obtained by using a set of different complex fault impedances at the POE. They illustrate the data used for the application of Method II in the identification of $\overline{I}_{vd}^{+}$ (3) using LOWESS. The surfaces show both real and imaginary parts of $\overline{I}_{vd}^{+}$ with respect to real and imaginary parts of the $\overline{V}_{f}^{+}$. In the application of LOWESS, the data is split into four windows, i.e., each window spans 25% of the total data.
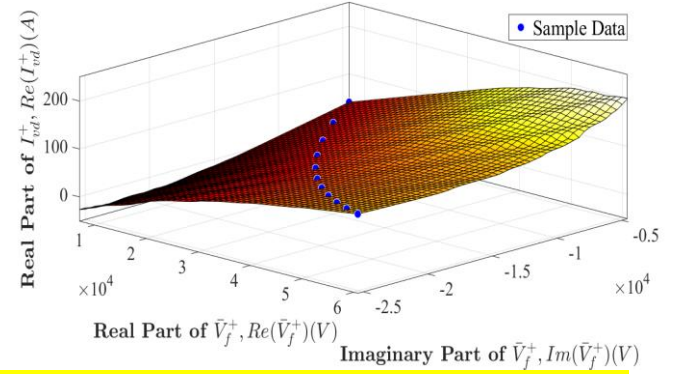

Fig 13 Real part of the current source versus real and imaginary parts of fault voltage
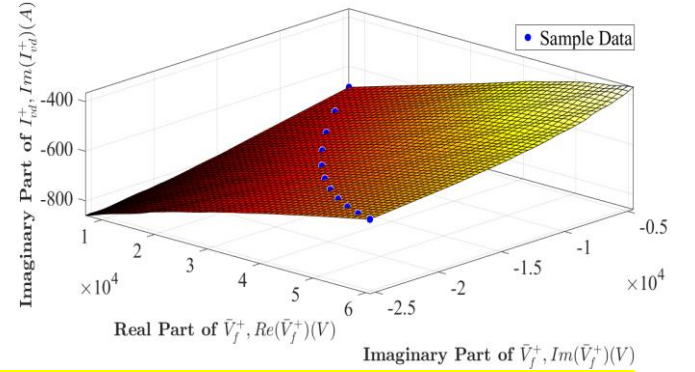

Fig 14 Imaginary part of the current source versus real and imaginary parts of fault voltage

B. Validation of the VDNE

Once all the parameters of the VDNE of the test system in Fig. 4 are identified, it is possible to test the performance of VDNE with both methods considering varying parameters for Z_{ext}.

TABLE II to TABLE IV show the performance of VDNE in computing the fault current following a three-phase-to-ground (3PH) fault applied at the POE considering Method I for $\overline{I}_{vd}^{+}$ identification. RMS fault current values are provided. The VDNE column represents the fault current computed using VDNE, which also includes the contribution of the external grid. In all studies the resistive part of the external grid's impedance is fixed to 5Ω and its X/R ratio is varied as illustrated in the first column of tables. The fault resistance is also varied as shown in Table captions.

The EMT simulations show slight oscillations in steady state short circuit conditions in the time domain. Average values are tabulated in this paper. This is considered as a factor contributing to the mismatch between the solutions obtained using EMT and VDNE. The highest error in percentage is 0.47 and observed for the lowest X/R ratio considered. In the parametric identification of VDNE, a fixed X/R ratio of 30 was considered. This explains increasing error as the ratio deviates from 30.

TABLE II
315 KV SYSTEM, 3PH FAULT, 1 OHM

X/R	Fault Current Comparisons				
	EMT (A)	VDNE (A)	EMT (°)	VDNE (°)	Error% in Magnitude
5	10168.27	10170.00	-76.24	-76.19	0.02
15	7112.45	7109.38	-78.42	-78.49	0.04
30	6103.31	6103.07	-78.16	-78.18	<0.01
50	5666.33	5668.27	-77.77	-77.73	0.03

TABLE III
315 KV SYSTEM, 3PH FAULT, 5 OHMS

X/R	Fault Current Comparisons				
	EMT (A)	VDNE (A)	EMT (°)	VDNE (°)	Error% in Magnitude
5	9584.02	9604.42	-66.11	-66.05	0.21
15	6953.53	6952.59	-72.09	-72.10	0.01
30	6016.57	6016.92	-73.18	-73.17	0.01
50	5601.53	5604.63	-73.39	-73.35	0.06

TABLE IV
315 KV SYSTEM, 3PH FAULT, 10 OHMS

X/R	Fault Current Comparisons				
	EMT (A)	VDNE (A)	EMT (°)	VDNE (°)	Error% in Magnitude
5	8480.11	8520.44	-54.34	-53.85	0.47
15	6503.39	6505.99	-63.44	-63.35	0.04
30	5714.59	5714.69	-65.97	-65.96	<0.01
50	5352.73	5354.34	-66.87	-66.87	0.03

C. Comparison with a Conventional Approach

The conventional network equivalent approach requires representing WPs with equivalent conventional generators. If the impedance of the generator is computed using the impedance of the circuit between the aggregated wind turbine and the POI, this will lead to very large overestimations in short circuit currents since the current limiters of VSCs will be ignored. This approach will not be considered for comparison purposes in this paper. One approach used in professional short circuit packages is to compute the impedance of the equivalent generator considering the current limit of VSCs which is set to 1.1 pu in this work. This method is not as accurate as the proposed VDNE approach since it does not consider the nonlinear voltage-dependent behavior of WPs. TABLE V shows the fault currents obtained using the equivalent generator model for WPs.

TABLE V
FAULT CURRENT USING EQUIVALENT CONVENTIONAL GENERATORS

Z_f (Ω)	EMT (A)/(Angle°)	Conventional (A)/(Angle°)	Error% in Magnitude
1	6103.31 (-78.16)	5850.50 (-78.01)	4.32
5	6016.57 (-73.18)	5661.80 (-70.97)	6.27
10	5714.59 (-65.97)	5342.40 (-63.11)	6.97

D. Comparison of Methods for Complex Fault Impedance

When three-phase-to-ground faults are applied with complex impedances, the VDNE obtained with Method I is not sufficient to provide accurate values for some of the simulated scenarios and therefore Method II is considered. TABLE VI compares the accuracies of Methods I and II considering various complex fault impedances for the test case under consideration. The maximum error in fault current magnitude encountered with Method II is 0.69% while it reaches up to 9.27% with Method

I. The extra dimension in the fitting formulation of Method II increases the accuracy in cases with complex fault impedances.

TABLE VI
COMPARISON BETWEEN METHODS I AND II FOR DIFFERENT COMPLEX FAULTS, 315KV SYSTEM, 3PH FAULT, X/R=30

Z_f (Ω)	EMT (A) (Angle°)	VNDE: Fault current calculation		Error% in Magnitude	
		Method I	Method II	Method I	Method II
j1	5863.99 (-79.05)	5366.32 (-70.92)	5873.34 (-79.21)	9.27	0.16
j5	5150.09 (-79.16)	4996.55 (-71.32)	5148.95 (-79.09)	3.07	0.02
j10	4491.01 (-79.74)	4538.67 (-72.71)	4461.08 (-78.97)	1.05	0.67
1+j1	5880.58 (-77.91)	5840.87 (-72.71)	5880.58 (-77.91)	0.68	<0.01
1+j5	5159.72 (-77.96)	5102.37 (-70.68)	5153.85 (-77.91)	1.12	0.11
1+j10	4495.25 (-78.58)	4572.32 (-71.87)	4464.31 (-77.90)	1.69	0.69
5+j1	5817.37 (-73.03)	5898.78 (-71.96)	5815.49 (-72.20)	1.38	0.03
5+j5	5130.37 (-73.18)	5291.36 (-69.00)	5130.39 (-73.18)	3.04	<0.01
5+j10	4475.22 (-74.03)	4642.95 (-68.96)	4461.17 (-73.99)	3.61	0.31
10+j1	5551.28 (-66.17)	5603.53 (-65.80)	5531.61 (-64.23)	0.93	0.36
10+j5	4965.27 (-67.11)	5131.38 (-65.14)	4952.61 (-66.34)	3.24	0.26
10+j10	4372.81 (-68.47)	4564.39 (-65.18)	4372.85 (-68.47)	4.20	<0.01

V. CONCLUSIONS

This paper has presented a first step towards identifying network equivalents of systems with high share of IBRs for short circuit studies. The proposed VDNE is a nonlinear equivalent and supplements the classic voltage source behind impedance representation by adding a nonlinear voltage dependent current source element. The computation of short circuit currents with the equivalent network needs to be done iteratively due to the nonlinear relationship between the fault contribution of the VDNE and the voltage at its terminals. This is the result of IBRs having different fault characteristics compared to SGs.

The application of the proposed model is tested by simulating various faults on a 315 kV multi-WP test system considering FSC topology for WTGs. The EMT simulation results of the complete network after reaching steady state in the time domain are taken as reference solution and compared with the proposed iterative solver employing the VDNE in the phasor domain. The initial results suggest an acceptable match between the solutions obtained with the VDNE and complete network.

In this work, the external grid is represented by a Thevenin equivalent. However, it can be modeled in detail and a fault can have an arbitrary location inside. In this case, it is important to identify the nonlinear current source component of the VDNE considering a large spectrum of impedance characteristics seen at the POE. A future work is the evaluation of the negative

sequence system considering flexible positive and negative sequence control strategies for WPs. Another future work is the standardization and optimization of the identification process of the voltage-dependent current source in the VDNE considering a variety of cases and IBR generation and integration scenarios.

VI. REFERENCES

[1] R. R. J. Nelson and H. Ma, "Short circuit contributions of full-converter wind turbines," *IEEE PES T&D Conference*, Orlando, FL, USA, May 2012.

[2] T. Kauffmann, U. Karaagac, I. Kocar, S. Jensen, J. Mahseredjian, and E. Farantatos, "An accurate type III wind turbine generator short circuit model for protection applications," *IEEE Trans. Power Del.,* vol. 32, no. 6, pp. 2370-2379, Dec. 2017.

[3] T. Kauffmann, I. Kocar, U. Karaagac, S. Jensen, and E. Farantatos, "Short-Circuit Model for Type-IV Wind Turbine Generators with Decoupled Sequence Control," *IEEE Trans. on Power Del.*, vol. 34, no. 5, pp. 1998-2007, Oct. 2019.

[4] T. Kauffmann, U. Karaagac, I. Kocar, H. Gras, J. Mahseredjian, B. Cetindag, and E. Farantatos, "Phasor Domain Modeling of Type III Wind Turbine Generator for Protection Studies," IEEE Power & Energy Society General Meeting, 2015.

[5] J. Morren and S. W. H. de Haan, "Short-circuit current of wind turbines with doubly fed induction generator," IEEE Trans. Energy Convers., vol. 22, no. 1, pp. 175–180, Mar. 2007.

[6] "Impact of inverter-based generation on bulk power system dynamics and short-circuit performance", PES-TR68, prepared by the IEEE/NERC Task Force on Short-Circuit and System Performance Impact of Inverter Based Generation, Jul. 2018.

[7] A. Haddadi, M. Zhao, I. Kocar, E. Farantatos, and F. Martinez, "Impact of Inverter-Based Resources on Memory-Polarized Distance and Directional Protective Relay Elements," 52nd North American Power Symposium (NAPS), 2021.

[8] A. Haddadi, I. Kocar, J. Mahseredjian, U. Karaagac, and E. Farantatos "Performance of Phase Comparison Line Protection under Inverter-Based Resources and Impact of the German Grid Code," IEEE Power & Energy Society General Meeting, 2020.

[9] A. Haddadi, M. Zhao, I. Kocar, U. Karaagac, K. W. Chan, and E. Farantatos, "Impact of Inverter-Based Resources on Negative Sequence Quantities-Based Protection Elements," accepted, in *IEEE Trans. on Power Del.*, Mar. 2020.

[10] System Protection Guidelines for Systems with Inverter Based Resources: Performance of Line Current Differential, Phase Comparison, Negative Sequence, Communication-Assisted, and Frequency Protection Schemes Under Inverter-Based Resources and Impact of German Grid Code. EPRI, Palo Alto, CA: 2019. 3002016196.

[11] I. Erlich, T. Neumann, F. Shewarega, P. Schegner, and J. Meyer, "Wind turbine negative sequence current control and its effect on power system protection,", *IEEE Power Energy Soc. Gen. Meeting*, Jul. 2013.

[12] Impact of Inverter-Based Resources on Power Swing and Rate of Change of Frequency Protection. EPRI, Palo Alto, CA: 2020. 3002016198.

[13] A. Haddadi, I. Kocar, U. Karaagac, and E. Farantatos, "Impact of Wind Generation on Power Swing Protection," in *IEEE Trans. on Power Del.*, vol. 34, no. 3, pp. 1118-1128, Jun. 2019.

[14] L. He, C. C. Liu, A. Pitto, and D. Cirio, "Distance protection of AC grid with HVDC-connected offshore wind generators," *IEEE Trans. Power Del.*, vol. 29, no. 2, pp. 493–501, Apr. 2014.

[15] S. Srivastava, A. Biswal, S. Ganesan, and U. J. Shenoy, "Behavior of self-polarized Mho characteristic on lines fed from DFIG based wind farms," *IEEE Innovative Smart Grid Technologies-Asia*, Bangalore, Nov. 10–13, 2013.

[16] M. Nagpal and C. Henville, "Impact of Power-Electronic Sources on Transmission Line Ground Fault Protection", *IEEE Trans. Power Del.*, vol. 33, no. 1, pp. 62–70, Feb. 2018.

[17] A. Hooshyar, M. A. Azzouz, and E. F. El-Saadany, "Distance protection of lines emanating from full-scale converter-interfaced renewable energy power plants–Part I: Problem statement," *IEEE Trans. Power Del.*, vol. 30, no. 4, pp. 1770–1780, Aug. 2015.

[18] A. Hooshyar, M. A. Azzouz, and E. F. El-Saadany, "Distance protection of lines emanating from full-scale converter-interfaced renewable energy power plants – Part II: Solution description and evaluation," *IEEE Trans. Power Del.*, vol. 30, no. 4, pp. 1781–1791, Aug. 2015.

[19] L.D. Bellomo, "Modelling of Wind Energy Converters for Slow and Fast Transients," Ph.D. dissertation, École Polytechnique de Montréal, QC, Canada, 2011.

[20] R. Teodorescu, M. Liserre, P. Rodriguez, Grid Converters for Photovoltaic and Wind Power Systems, 2011, IEEE/Wiley.

[21] Modification of Commercial Fault Calculation Programs for Wind Turbine Generators, System Protection Subcommittee, WG C24.

[22] U. Karaagac, J. Mahseredjian, R. Gagnon, H. Gras, H. Saad, L. Cai, I. Kocar, A. Haddadi, E. Farantatos, S. Bu, K. W. Chan, L. Wang, "A Generic EMT-type Simulation Model for Wind Parks with Full Size Converter Wind Turbines," in *IEEE Power and Energy Technology Systems Journal*, vol. 6, no. 3, pp. 131-141, Sep. 2019.

[23] "Grid code - high and extra high voltage," E.ON Netz GmbH, Bayreuth, Germany, April 2006.

[24] R. Gagnon *et al.*, "Hydro-Québec Strategy to Evaluate Electrical Transients Following Wind Power Plant Integration in the Gaspésie Transmission System," in *IEEE Transactions on Sustainable Energy*, vol. 3, no. 4, pp. 880-889, Oct. 2012.

[25] L. Xu and Y. Wang, "Dynamic Modeling and Control of DFIG-Based Wind Turbines Under Unbalanced Network Conditions," in IEEE Transactions on Power Systems, vol. 22, no. 1, pp. 314-323, Feb. 2007.

[26] J. Hu and Y. He, "Reinforced Control and Operation of DFIG-Based Wind-Power-Generation System Under Unbalanced Grid Voltage Conditions," in *IEEE Transactions on Energy Conversion*, vol. 24, no. 4, pp. 905-915, Dec. 2009.

[27] Y. Chang, J. Hu, W. Tang and G. Song, "Fault Current Analysis of Type-3 WTs Considering Sequential Switching of Internal Control and Protection Circuits in Multi Time Scales During LVRT," in *IEEE Transactions on Power Systems*, vol. 33, no. 6, pp. 6894-6903, Nov. 2018.

[28] Y. Chang, J. Hu and X. Yuan, "Mechanism Analysis of DFIG-Based Wind Turbine's Fault Current During LVRT With Equivalent Inductances," in *IEEE Journal of Emerging and Selected Topics in Power Electronics*, vol. 8, no. 2, pp. 1515-1527, June 2020.

[29] Á Björck and V. Pereyra. "Solution of Vandermonde systems of equations." Mathematics of computation v.24 n.112 pp.893-903, Oct. 1970

[30] W. S. Cleveland, "Robust locally weighted regression and smoothing scatterplots", in *Journal of the American statistical association*, Vol. 74, No. 368, pp. 829- 836, Dec. 1979.